Blind Deblurring of Spiral CT Images

Ming Jiang*
School of Mathematics
Peking University
Beijing 100871, China.

Ge Wang
Department of Radiology
University of Iowa
Iowa City, IA 52242, USA

Margaret W. Skinner
Department of Otolaryngology
Washington University
Saint Louis, MO 63110, USA

Jay T. Rubinstein
Department of Otolaryngology
University of Iowa
Iowa City, IA 52242, USA

Michael W. Vannier
Department of Radiology
University of Iowa
Iowa City, IA 52242, USA

November 2, 2001

Abstract

The temporal bone is a complex paired set of structures at the skull base which contains the organ of hearing among others [1]. Treatment of severe to profound, bilateral hearing loss often employs a multi-electrode cochlear implant inserted into the inner ear part of the temporal bone. CT scanners cannot resolve many important temporal bone details, especially bony anatomy. We improve the high-contrast spatial resolution of CT with blind deblurring of CT slices and tested the improvement using a phantom test object. The improvement in visible detail or clinic scans is apparent subjectively and approaches 33% quantitatively.

1 Introduction

Spiral/helical computed tomography (CT) is advantageous in visualizing and measuring bony structures. However, CT scanners cannot resolve many important temporal bone details, especially those millimeter or sub-millimeter sized structures of the middle and inner ear. In this paper, we developed a blind deblurring algorithm to improve the high-contrast spatial resolution of CT sections.

Spiral CT can be modeled as a spatially invariant linear system with a 3D Gaussian point spread function (PSF) that is separable and nearly isotropic [2]. As a result, an arbitrary oblique cross-section in an image volume can then be approximated as the convolution

$$g(x) = p(x) \otimes \lambda(x), \tag{1}$$

where $p(x) = G_\sigma(x)$ is the 2-D Gaussian function with standard deviation σ, $g(x)$ is the chosen oblique section, also referred to as the blurred image, and $\lambda(x)$ is the actual cross-section, i.e., the real image. An estimate of the real image is called a restored or deblurred image.

If the parameter σ was known, the EM deblurring algorithm [3] was used to find the deblurred image in [2]. The EM algorithm is well established and has been successfully used in many different applications. For the imaging model (1), the EM algorithm iterates as follows:

$$\lambda_{k+1} = \lambda_k \cdot \left[\bar{p} \otimes \left(\frac{g}{p \otimes \lambda_k}\right)\right] \tag{2}$$

where $\bar{p}(x) = p(-x)$ and λ_k is the deblurred image at iteration k.

If the standard deviation σ is unknown, that is our case for an arbitrary oblique cross-section, a blind deblurring/deconvolution algorithm can be used to find the deblurred image and improve image resolution. Blind deblurring can restore a blurred image without prior determination of the PSF. Essentially, we need a good estimate of the standard deviation σ.

Blind deblurring was recently reviewed [4, 5]. However, all the blind deblurring methods reviewed in [4, 5] require that the PSF and the original image must be *irreducible*. An irreducible signal cannot be exactly expressed as the convolution of two or more component signals of the same family. However, this fundamental assumption is invalid for the Gaussian PSF.

Existing algorithms for Gaussian blind deblurring are not very successful. One popular method is the double iteration scheme developed by Holmes *et al.*

*Currently, Ming Jiang is a visiting professor with Micro-CT Laboratory, Department of Radiology, University of Iowa, Iowa City, IA 52242, USA.

0-7803-7147-X/01/$10.00©2001 IEEE

[6]. The major disadvantages of the double iteration method are: (1) no convergence proof of this method; (2) the result depends on the initial values. With an inappropriate initial guess, the PSF p_k may converge to a δ function and the deblurred image can be just the observed image g [7]!

The paper is organized as follows. In § 2, an edge-to-noise ratio is defined and a novel blind deblurring algorithm is proposed to find the standard deviation σ by optimizing this edge-to-noise ratio. § 3 introduces the phantom and practical patient data used in this study. In § 4, we report results from numerical simulation and patient studies. In § 5, we discuss relevant issues and future refinements of the methodology, and conclude the paper.

2 Methods

2.1 Edge-to-Noise Ratio

Our work is based on Snyder *et al.* [8], where for the EM deblurring algorithm (2) with a Gaussian blurring kernel,

- *"The overshoot(at edges) is seen to be a weak function of the sieve; in general, the overshoot increases slightly with wider sieves."*
- *"The overshoot is a strong function of the resolution width; the overshoot decreases rapidly as the resolution-kernel width is increased."*
- *"The overshoot increases with iteration number."*

The deblurring, resolution and sieve widths are the standard deviations of different Gaussians, which are related as follows:

$$\sigma^2 = \sigma_0^2 + \sigma_S^2 - \sigma_R^2 \tag{3}$$

where σ is the deblurring width, σ_0 the real blurring width, σ_S and σ_R are the sieve and resolution widths, respectively. Because increasing the sieve width is equivalent to increasing the deblurring kernel width, and increasing the resolution width is equivalent to decreasing the deblurring kernel width, the the overshoot increases as the deblurring kernel width increases. The overshoot is a combination of the noise and edge effects when the data is corrupted with noise.

To quantify those two effects, we use the axiomatic discrepancy measure developed in [9]. For two non-negative distributions u and v, the only discrepancy measure consistent with Csiszár's axioms [9] is the I-divergence, or generalized Kullback distance

$$I(u,v) = \sum_x u(x) \log \frac{u(x)}{v(x)} - \sum_x [u(x) - v(x)] \tag{4}$$

The noise effect is considered as the discrepancy of the observed blurred data and the mean value of it. The mean value of the blurred image is estimated as $G_\sigma \otimes \lambda_{\mathrm{EM}}(g,n,\sigma)$ where $\lambda_{\mathrm{EM}}(g,n,\sigma)$ is a deblurred image by the EM algorithm with n iterations and deblurring σ. The noise effect for a deblurring σ by the EM algorithm with n iterations is then defined as

$$N(\sigma,n) = I(g, G_\sigma \otimes \lambda_{\mathrm{EM}}(g,n,\sigma)) \tag{5}$$

Another discrepancy appears naturally by considering the deblurred image $\lambda_{\mathrm{EM}}(g,n,\sigma)$ and the estimated mean value $G_\sigma \otimes \lambda_{\mathrm{EM}}(g,n,\sigma)$ of the blurred image g:

$$E(\sigma,n) = I(\lambda_{\mathrm{EM}}(g,n,\sigma), G_\sigma \otimes \lambda_{\mathrm{EM}}(g,n,\sigma)) \tag{6}$$

This is termed as the *measure of deblurring* for a deblurring σ by the EM algorithm with n iterations. This measures the enhancement of edges after restoration.

$E(\sigma,n)$ measures not only the edge effect but also includes part of the noise effect. Hence, the net edge effect may be approximated by $E(\sigma,n) - kN(\sigma,n)$, where $kN(\sigma,n)$ represents a certain amount of the noise effect inclueded in $E(\sigma,n)$ and k is a positive weighting constant.

Choosing σ by simply maximizing $E(\sigma,n) - kN(\sigma,n)$ to achieve edge enhancement may result in a deblurred image with exaggerated edges and unacceptable noise effect, since the noise effect is not controlled in the object function. Hence, we need a balance between the edgeness improvement $(E(\sigma,n) - kN(\sigma,n))$ and the noise magnification $(N(\sigma,n))$. This consideration leads to the following "edge-to-noise" ratio:

$$\mathrm{ENR}(\sigma,n) = \frac{E(\sigma,n) - kN(\sigma,n)}{N(\sigma,n)} \tag{7}$$

Consequently, we have the following

ENR Principle: *Given n, the deblurring σ should be so chosen such that the deblurred image maximizes $ENR(\sigma,n)$.*

Since maximizing $\mathrm{ENR}(\sigma,n)$ is equivalent to maximize $\frac{E(\sigma,n)}{N(\sigma,n)}$, we can simply use the latter and eliminate the need for the unknown weighting constant k. This leads us to define

$$\mathrm{DNR}(\sigma,n) = \frac{E(\sigma,n)}{N(\sigma,n)} \tag{8}$$

which is termed simply as the deblurring to noise ratio. Hence, we can refine our basic criteria as

DNR principle: *Given n, the optimal deblurring σ for producing the optimal deblurred image will be the one that maximize $DNR(\sigma,n)$.*

2.2 Blind Deblurring Algorithm

The searching for the optimal deblurring σ value can be formulated as a one-dimensional maximization problem. Since the definition of the DNR depends on the iteration number n, the choice of the iteration number n is important to find an optimal estimate of the deblurring σ. The optimal iteration number depends on the image content and can be found for a class of images through simulation and/or experiments using an appropriately designed phantom. This is demonstarted in § 4.2, where we use an image fidelity evaluation to determine the optimal EM iteration number because the real image is available.

Our algorithm is described as follows:

Step 1 Initialization: Take DNR$(\cdot)$ as the object function for maximization, determine an EM iteration number n from phantom experiments, and determine an bracket interval $[\sigma_{\min}, \sigma_{\max}]$ for the permissible σ values;

Step 2 Estimation: using a one-dimensional optimization algorithm to find the maximum point σ;

Step 3 Restoration: With σ obtained in Step 2 as the deblurring σ, use the EM algorithm (2) to find the actual cross-section.

In the above algorithm, the one-dimensional optimization algorithm is left for the user to choose. There are some sophisticated algorithms for this task. In this work, we use the MatLab function "**fminbnd()**", which is a combination of golden section search and parabolic interpolation. The 3rd step could be saved if it is already computed in the 2nd step.

3 Materials

3.1 Phantom of the Cochlea

Since our main interest is to deblur sectional temporal bone CT images, we rely on an idealized cross-section of the human cochlea Figure 1, which is described as follows. Decalcified and celloidin embedded, grossly normal, right temporal bones from two adults were serially sectioned, one horizontally and the other vertically. The sections were then stained with hematoxylin and eosin. A midmodiolar section from each cochlea was projected at 40 times onto a drawing paper and a tracing of the three main structures was made: the cochlea scalae, soft tissue and bone. A transparent, precision ruler (0.5 millimeter) was then projected onto the paper, and the tick marks were traced to show the magnification factor. The drawings were then digitally scanned and scaled to 0.1 millimeter square pixels, and combined into one image of 100 by 100 pixels. Mean CT numbers for fluid (perilymph and endolymph in the cochlear scale), soft tissue and bone were estimated from real spiral CT scans as -443, 214 and 2384 HU respectively, and then assigned to corresponding classes in the combined image.

Figure 1: Phantom of the cochlea.

3.2 Patient Data

The patient was scanned using a Toshiba Xpress/SX spiral CT scanner (Toshiba Corp., Tokyo, Japan). The imaging protocol was 1 mm collimation and 1 mm table feed per gantry rotation. Images were reconstructed via half-scan interpolation at 0.1 mm longitudinal interval. In reconstruction, a 18 cm field of view (FOV) was used, which was later restricted to a 51 mm FOV via direct reconstruction. As a result, the in-plane square pixel size is 0.1 mm.

4 Results

In this section, we first demonstrate the property of the proposed DNR as a function of σ and n by numerical simulation with the phantom and experimentally validate the DNR principle. Then we use the root mean square error(RMSE) as a measure of image fidelity to determine the optimal iteration number n for our application. The patient study is given in § 4.3.

4.1 Validation of DNR Principle

This is done by plotting the graph of the function DNR$(\cdot, n)$ through heavy numerical computation:

1. For σ_0 ranging from 0.1mm to 0.5mm with step length 0.05mm, the phantom of the cochlea is blurred with PSF G_{σ_0}. The result is $I(\sigma_0)$;

2. Each blurred image $I(\sigma_0)$ is further degraded with the Poisson noise. The result is $g(\sigma_0)$;

3. Each blurred image $g(\sigma_0)$ is deblurred by the EM algorithm with deblurring σ from 0.08mm to 0.6mm in steps of 0.005mm and iteration number n from 10 to 200 in steps of 5. The result is $\lambda(\sigma, g(\sigma_0), n)$;

4. The DNR values at those σ and n are computed, the result is $\text{DNR}(\sigma, n)_{\sigma_0}$.

5. The DNR values computed is plotted.

Fig. 1 is the DNR profile for $\sigma_0 = 3$mm and $n = 20$. As shown in Fig. 1, the plotted $\text{DNR}(\sigma, n)_{\sigma_0}$ validates the DNR principle for the estimation of the real blurring σ_0: it possesses a unique maximum in the interval given, and the maximizer is close to the real σ_0. The

same can be found for other real blurring σ_0 values in the above defined range. For brevity, other profiles are not included.

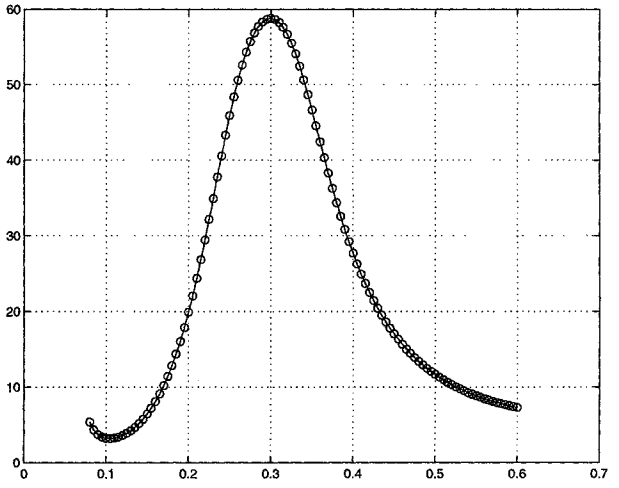

Figure 2: DNR profile with respect to σ for $\sigma_0 = 0.3$ and $n = 20$.

4.2 Find the Optimal n

The optimal iteration number n is determined such that the image fidelity improvement is the best if the image is deblurred by a σ estimated by DNR principle with this n, as follows:

1. Use the result in § 4.1, i.e., those computed $\text{DNR}(\sigma, n)_{\sigma_0}$ values;

2. For each image $g(\sigma_0)$ and n from 10 to 200 in steps of 5, find the σ value within $[0.08, 0.6]$ discretized in steps of 0.005mm that maximize $\text{DNR}(\sigma, n)_{\sigma_0}$. The result is $\sigma(\sigma_0, n)$.

3. The root mean square error(RMSE) of the deblurred image $\lambda(\sigma, g(\sigma_0), n)$ with $\sigma = \sigma(\sigma_0, n)$ and the real phantom image is computed. The RMSE is defined as follows:

$$\text{RMSE}(A, B) = \sqrt{\frac{1}{N}\sum_x (A(x) - B(x))^2}. \quad (9)$$

4. The improvement of image fidelity in RMSE after deblurring is then computed, which is defined as the percentage of change $\beta(n)$ after deblurring:

$$\beta(\sigma_0, n) = \frac{\text{RMSE}(g(\sigma_0), I) - \text{RMSE}(\lambda, I)}{\text{RMSE}(\lambda, I)}\% \quad (10)$$

where n denotes the iteration number, I is the original image phantom and $\lambda = \lambda(\sigma, g(\sigma_0), n)$.

Table 1 lists the improvement in percentage obtained from deblurring experiments using the phantom of the cochlea, and $n = 25, 30, 35, 40, 45, 50$. The last row is the average of the improvement. The iteration number n that gives the best improvement is chosen as the iteration number in the blind deblurring algorithm.

Table 1: RMSE Improvement

σ_0	rmse	$\beta(25)$	$\beta(30)$	$\beta(35)$	$\beta(40)$	$\beta(45)$	$\beta(50)$
0.10	3.02	45%	47%	44%	44%	44%	44%
0.15	3.78	38%	41%	40%	41%	42%	37%
0.20	4.37	34%	36%	36%	38%	36%	37%
0.25	4.90	30%	30%	28%	26%	22%	23%
0.30	5.37	25%	24%	22%	19%	18%	18%
0.35	5.79	29%	27%	26%	25%	23%	20%
0.40	6.19	31%	31%	31%	30%	29%	28%
0.45	6.55	29%	30%	32%	31%	31%	31%
0.50	6.88	27%	28%	29%	30%	30%	31%
mean		32%	33%	32%	32%	31%	30%

It can be observed in Table 1 that $n = 30$ could yield the best image fidelity improvement.

4.3 Patient Study

In the patient study, the initial interval of σ is selected to be $[0.08, 0.60]$, which contains possible σ_0 values, based on the specification of the CT scanner and our experience with CT quality assurance [2]. The blind deblurring algorithm of § 2.2 consistently produces excellent deblurring results. As shown in Fig. 3 and Fig. 4, anatomical features are substantially clarified.

5 Conclusion

To apply our blind deblurring algorithm, we should first address two important issues: (1) a range of the blurring σ, (2) an iteration number. The range of the blurring σ can be estimated based on the system MTF and data from CT quality assurance tests [2] (also the references therein). The optimal EM iteration number can be determined in simulation and experiments using a representative phantom.

In conclusion, we have developed a blind deblurring algorithm to improve spiral CT image resolution for cochlear implantation. This algorithm is based on a powerful edge-to-noise ratio concept, which characterizes the image quality improvement due to deblurring. We have evaluated and validated this blind deblurring methodology in the Gaussian blurring case, and demonstrated the utility in the phantom experiment and patient study.

Figure 3: Original 300 × 200 CT Image through the basal turn of the cochlea.

Figure 4: Deblurred with estimated deblurring $\sigma = 4.1343$ and $n = 30$.

Acknowledgments

This work is supported by an NIH grant(R01 DC03590). The authors are also grateful to Troy Frei, from the Department of Radiology, University of Iowa, for preparing the data for validating the Gaussian PSF for a multi-row detector CT scanner.

References

[1] M. W. Vannier and G. Wang, "Spiral CT refines temporal bone imaging," *Diagnostic Imaging*, vol. 15, pp. 116 – 121, 1993.

[2] G. Wang, M. W. Vannier, M. W. Skinner, M. G. P. Cavalcanti, and G. Harding, "Spiral CT image deblurring for cochlear implantation," *IEEE Trans. Medical Imaging*, vol. 17, pp. 251 – 262, 1998.

[3] D. L. Snyder, T. J. Schulz, and J. A. O'Sullivan, "Deblurring subject to nonnegativity constraints," *IEEE Trans. Signal Processing*, vol. 40, pp. 1143 – 1150, 1992.

[4] D. Kundur and D. Hatzinakos, "Blind image deconvolution," *IEEE Signal Processing Magazine*, vol. 13, no. 3, pp. 43 – 64, May 1996.

[5] D. Kundur and D. Hatzinakos, "Blind image deconvolution revisited," *IEEE Signal Processing Magazine*, vol. 13, no. 6, pp. 61 – 63, November 1996.

[6] T. J. Holmes, "Blind deconvolution quantum-limited incoherent imagery: maximum-likelihood approach," *J. Opt. Soc. Am. A*, vol. 9, pp. 1052 – 1061, 1992.

[7] F. Tsumuraya, N. Miura, and N. Baba, "Iterative blind deconvolution method using lucy's algorithm," *Astronomy and Astrophysics*, vol. 282, pp. 699 – 708, 1994.

[8] D. L. Snyder, M. I. Miller, L. J. Thomas, and D. G Politte, "Noise and edge artifacts in maximum-likelihood reconstructions for emission tomography," *IEEE Trans. Medical Imaging*, vol. 6, pp. 228 – 238, 1987.

[9] I. Csiszár, "Why least squares and maximum entropy? An axiomatic approach to inference for linear inverse problems," *The Annals of Statistics*, vol. 19, no. 4, pp. 2032 – 2066, 1991.